INFACON 7, Trondheim, Norway, June 1995
Eds.: Tuset, Tveit and Page
Publishers: FFF, Trondheim, Norway

A NUMERICAL MODEL FOR THE AC ARC IN THE SILICON METAL FURNACE

Hilde Løken Larsen, Gu Liping and Jon Arne Bakken
Department of Metallurgy,
The Norwegian Institute of Technology
Trondheim, NORWAY

ABSTRACT

Time-dependent numerical simulations have been carried out for an alternating current (AC) free-burning arc in a silicon metal furnace. The crater gas consists of Si-O-C compounds, and the arc burns between a graphite electrode and a silicon melt. The conservation equations for mass, momentum and energy together with the time-dependent Maxwell equations are solved. In addition the external electric circuit consisiting of an ideal voltage source representing the transformer secondary voltage, a lumped resistance and a lumped inductance is incorporated in the model. The total arc voltage and current, the current density distribution, the temperature, pressure and velocity fields are calculated as functions of time. Calculations are carried out for different sets of model input parameters, and the results are compared with current and power measurements on a real furnace. The effect of turbulence is also considered.

INTRODUCTION

The submerged electric arcs, burning in the gas filled craters of the furnace, supply the energy needed for the production of silicon metal. Although some of the electric current probably passes through the charge, estimates indicate about 10%, the main part of the electric power is dissipated in the arc and transferred by radiation, convection and electron impact to the metal bath and crater walls. Silicon metal has been produced for decades, but the crater processes are still not fully understood due to the practical difficulties in observing the reactions taking place and the behaviour of the arc in the crater. Models of the the crater /1/, the furnace shaft /2/ and the chemical reactions /3/ have been developed in order to increase process understanding and, if possible, optimize furnace operation. In addition, electric furnace models have been established with the purpose of describing the electrical conditions /4/. The arc is then included as a non-linear current-dependent resistance which must be given as an input parameter in the model. Because of the crucial role of the arc as an energy supplier, a physically realistic model of the electric arc can contribute to further development of the above mentioned type of models and increase the total knowledge of the process.

Channel models have previously been used for simulating industrial AC arcs (10 - 100 kA) /5/ and has also been implemented in models describing the electrical conditions /6/ in the

furnace. The arc is then treated as a cylindrical conductor with uniform temperature and current density. This is in contrast to the real situation with strong gradients in the arc. The model presented here is supposed to give a more correct picture of the arc and has already been applied on arcs with currents of about 1000 A /7/. Even with a fast computer, however, the CPU time required makes this model unsuitable for on-line use. An improved version of the channel model, which can be run on a standard PC, could perhaps be developed on the basis of the complex arc model described in this paper.

PRESENTATION OF THE MODEL

Modelling domain and assumptions

Typical dimensions of one of the three craters of a 22 MW furnace at the Elkem Fiskaa plant, Norway are shown on Figure 1 together with the modelling domain. A non-uniform 100×100 grid is used with the finest mesh in front of the graphite electrode and the metal bath, i.e. the areas where the strongest gradients in temperature, velocity etc. are expected to occur.

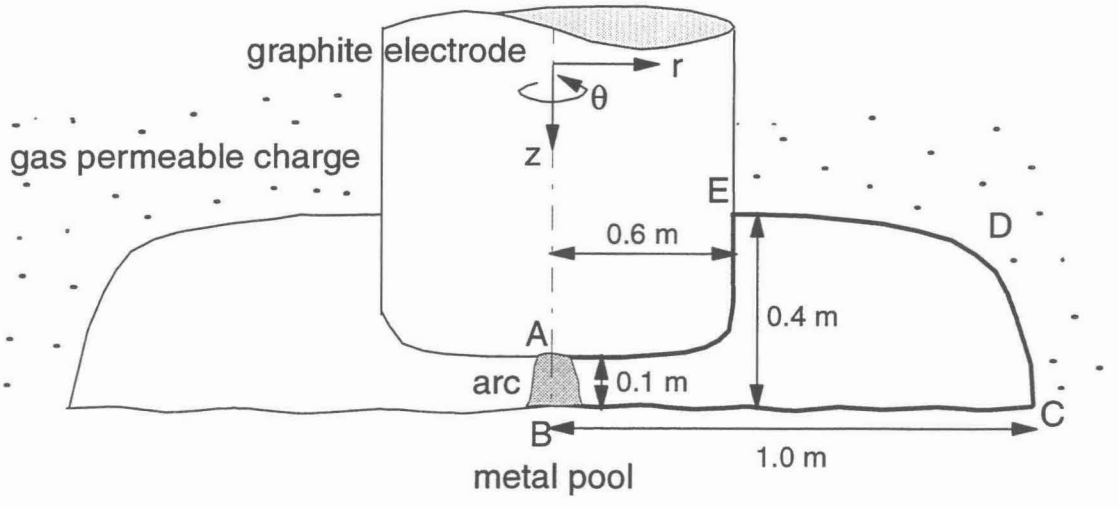

Figure 1 *Sketch of the silicon furnace crater and the modelling domain A-B-C-D-E*

The arc is assumed to be *cylidrically symmetric*. *Local thermal equlibrium* (LTE), which implies that the electron and the heavy particle temperatures are equal, is assumed in the plasma column. The near-electrode sheaths, where this assumption is known not to be valid, are therefore represented in the model by anodic and cathodic voltage falls.

Governing equations

In order to calculate the temperature, current densitiy, velocitiy, magnetic field and pressure distributions in the arc the *time-dependent* conservation equations for mass, energy and momentum must be solved together with Maxwell's equations for the electromagnetic field. The conservation equation for *mass* is

$$\frac{\partial \rho}{\partial t} + \frac{1}{r}\frac{\partial}{\partial r}(r\rho v_r) + \frac{\partial}{\partial z}(\rho v_z) = 0 \qquad (1)$$

where ρ is the density. v_r and v_z are the radial and axial velocities.

The *momentum* equations in radial and axial direction are

$$\frac{\partial(\rho v_r)}{\partial t} + \frac{1}{r}\frac{\partial}{\partial r}(r\rho v_r v_r) + \frac{\partial}{\partial z}(\rho v_z v_r) = -\frac{\partial p}{\partial r} + \frac{2}{r}\frac{\partial}{\partial r}(r\mu\frac{\partial v_r}{\partial r}) + \frac{\partial}{\partial z}\left(\mu(\frac{\partial v_r}{\partial z} + \frac{\partial v_z}{\partial r})\right) - \frac{2\mu v_r}{r^2} - j_z B_\theta \qquad (2)$$

$$\frac{\partial(\rho v_z)}{\partial t} + \frac{1}{r}\frac{\partial}{\partial r}(r\rho v_r v_z) + \frac{\partial}{\partial z}(\rho v_z v_z) = -\frac{\partial p}{\partial z} + \frac{\partial}{\partial z}(2\mu\frac{\partial v_z}{\partial z}) + \frac{1}{r}\frac{\partial}{\partial r}\left(r\mu(\frac{\partial v_r}{\partial z} + \frac{\partial v_z}{\partial r})\right) + j_r B_\theta \qquad (3)$$

where p is the pressure and the terms $F_r = -j_z B_\theta$ and $F_z = j_r B_\theta$ are the components of the *electromagnetic* force. Because of arc contraction near the cathode a radial current density, j_r, will occur there and give rise to an axial force which produces a flow towards the anode. The magnetic field is generated by the axial current, j_z, and has only an azimuthal component B_θ. The *energy* equation is

$$\frac{\partial(\rho h)}{\partial t} + \frac{1}{r}\frac{\partial}{\partial r}(r\rho v_r h) + \frac{\partial}{\partial z}(\rho v_z h) = \frac{\partial}{\partial z}(\frac{k}{c_p}\frac{\partial h}{\partial z}) + \frac{1}{r}\frac{\partial}{\partial r}\left(r\frac{k}{c_p}\frac{\partial h}{\partial r}\right) + \frac{j_z^2 + j_r^2}{\sigma} + \frac{5k_B}{2e}\left(\frac{j_z}{c_p}\frac{\partial h}{\partial z} + \frac{j_r}{c_p}\frac{\partial h}{\partial r}\right) - S_r \qquad (4)$$

where h is the specific enthalpy, k is the thermal conductivity, c_p is the specific heat, σ is the electric conductivity, k_B is Boltzmann's constant and e is the electronic charge. The joule heating term, the energy transported by electrons and the radiation term, S_r, are included as source terms.

From Maxwell's equations and the generalized Ohm's law $\boldsymbol{j} = \sigma(\boldsymbol{E} + \boldsymbol{v}\times\boldsymbol{B})$ the transport equation for *the magnetic field* B_θ is deduced:

$$\frac{\partial B_\theta}{\partial t} + \frac{1}{r}\frac{\partial}{\partial r}(rv_r B_\theta) + \frac{\partial}{\partial z}(v_z B_\theta) = \frac{\partial}{\partial r}\left(\frac{\Gamma_m}{r}\frac{\partial}{\partial r}(rB_\theta)\right) + \frac{\partial}{\partial z}\left(\Gamma_m\frac{\partial B_\theta}{\partial z}\right) \qquad (5)$$

The form of this equation is seen to be analog to the other conservation equations with an accumulation term, a convection term and a diffusion term. The magnetic diffusion coefficient is $\Gamma_m = (\mu_0\sigma)^{-1}$, where μ_0 is the permeability of vacuum. In order to estimate the effect of *turbulence*, the ordinary k-ε model with standard coefficients is applied in one of the calculations /8/. The viscosity in the momentum equations will then include the turbulent viscosity term: $\mu + \mu_t$. The transport coefficient in the entalphy equation will be modified to $k/c_p + \mu_t/Pr_t$.

The coupled set of differential equations presented above are solved by using a modified version of the commercial fluid flow and heat transfer programme FLUENT /8/ on a HP9000/755 computer. A time step of 0.01 ms was used in the calculations. One 50 Hz period thus corresponds to 2000 time steps. The final periodic solution is obtained after about two AC periods and is independent of the choice of DC starting solution at t = 0 /7/. The CPU time required for simulating one AC period is typically ~ 20 hours.

Boundary conditions

The boundary conditions for the modelling domain presented in Figure 2 are listed in Table 1. Symmetry conditions are used along the axis AB. The velocity at all walls is zero. The temperature on the crater walls is set to 2000 K /3/. The cathode will alternate between the graphite electrode and the silicon melt. Due to lack of information on electron emission from liquid silicon the metal bath is in practice treated as graphite. A parabolic current density

distribution is assumed on *the cathode* with a mean current density ranging from $j_c=0.5\cdot10^7$ to $2.0\cdot10^7 A/m^2$ in the different simulations. The corresponding electrode temperatures found from Richardson-Dushman's equation for thermionic electron emission /9/ are 3830 - 4180K. An electrode temperature of 4000 K is therefore used in all the simulations. The boundary conditions for the magnetic field on the electrode will change when the polarity of the current changes. In the cathodic half period the current density of the electrode is given and thereby also the magnetic field. In the anodic half period the radial current component, j_r, at the anode must be zero because the flat anode is an equipotential surface. From Maxwell's equation $\nabla\times\boldsymbol{B}=\mu_0\,\boldsymbol{j}$ it follows that $j_r = \partial B_\theta/\partial z = 0$. On the other surfaces the magnetic field is calculated from the analytical expression $B_\theta(r) = \mu_0 I/(2\pi r)$ of Ampere's law.

TABLE 1 *Boundary conditions for the equations (1)-(5)*

Domains (see Fig.1)	v_z	v_r	h	B_θ
AB	$\partial v_z/\partial r = 0$	0	$\partial h/\partial r = 0$	0
BC	0	0	4000 K	Anode: $\partial B_\theta/\partial z = 0$ Cathode: $B = B_{calc.}$
CD	0	0	2000 K	$B_\theta(r)$
DE	0	0	2000 K	$B_\theta(r)$
EA	0	0	4000 K	Anode: $\partial B_\theta/\partial z = 0$ Cathode: $B = B_{calc.}$

Transport coefficients and radiation data

The gas mixture in the crater consists of *silicon*, *oxygen* and *carbon*. The silicon to carbon-ratio of this gas mixture may in average be as defined by the SiO/CO-ratio required for liquid silicon to form with a realistic recovery in the crater. According to an analysis of the process given by Schei and Larsen /3/ this ratio may vary between 2 at 55% recovery to nearly 1 at 100% recovery provided that a reactive carbon material is used.

Calculated transport coefficients and thermodynamic properties are available for both gas mixtures /10/. The examples in Figure 2 (p = 1 bar) show that the properties are almost identical for the two gas mixtures. Argon, which is shown in the same figures for comparison, has also roughly similar data. An exception is the enthalpy which is higher for Si-O-C. Figure 3 shows that the properties are not only depending on temperature, but also on pressure. The radiation properties of argon are also pressure dependent as seen in Figure 4. Radiation data for Si-O-C gas mixtures are, however, not yet available. For this reason, transport coefficients, thermodynamic properties and radiation data for *argon* at 1 bar are used in the preliminary calculations on industrial high current arcs presented here.

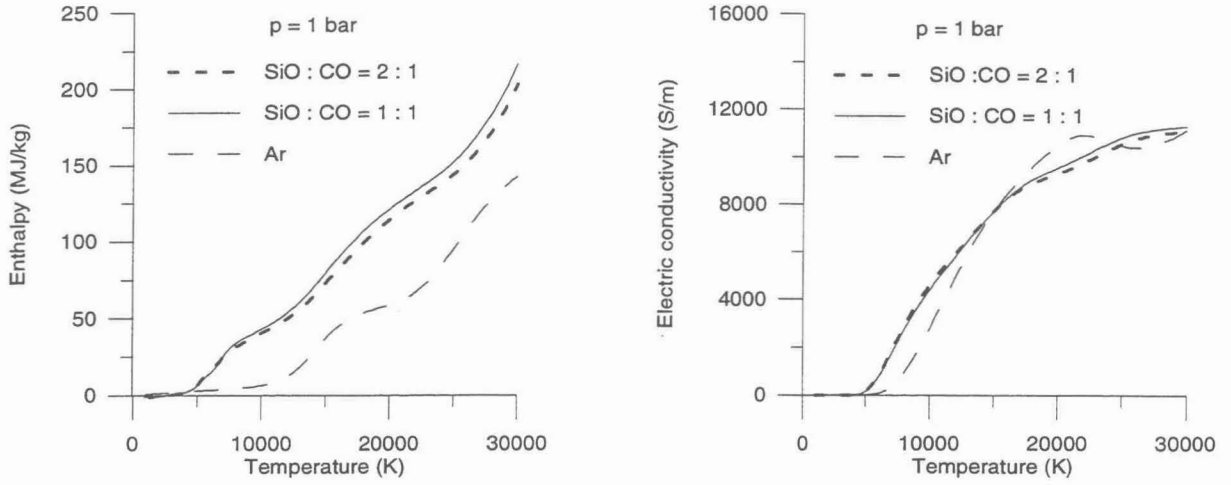

Figure 2 *a) Enthalpy and b) electric conductivity for Si-O-C mixtures and argon (p = 1 bar)*

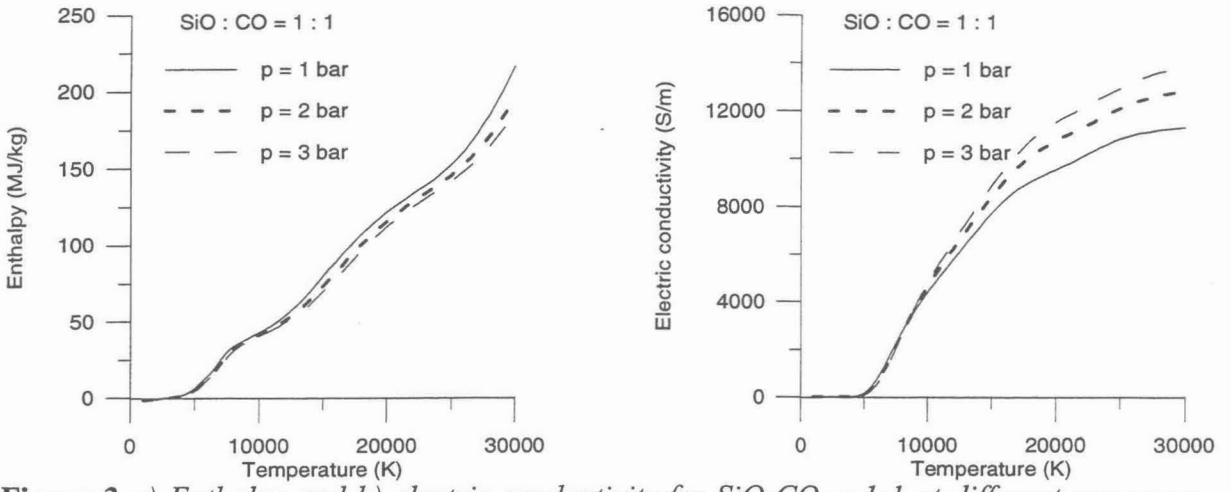

Figure 3 *a) Enthalpy and b) electric conductivity for SiO:CO = 1:1 at different pressures*

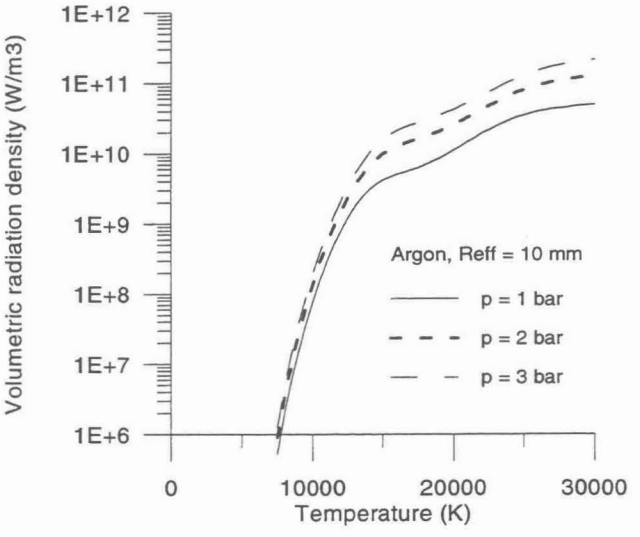

Figure 4 *Volumetric radiation density (W/m^3) for Argon at different pressures (effective radiation radius = 10 mm)*

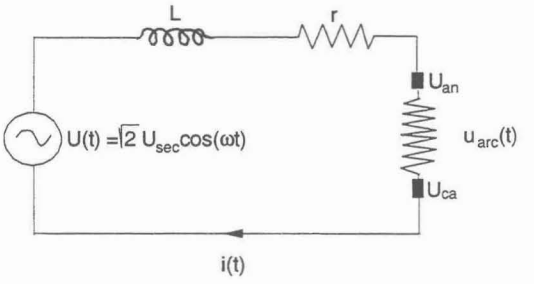

Figure 5 *The electric circuit*

The electric circuit

The momentaneous current in the arc is calculated by taking the electric circuit - in which the arc is a non-linear circuit element - into account. As shown in the single-phase diagram in Figure 5, the circuit consists of an ideal voltage source representing the transformer secondary phase voltage U_{sec}, a phase resistance r representing the ohmic losses in the transformer, current cables etc. and a phase inductance L. Elkem Fiskaa has provided typical parameters for a 22 MW three-phase silicon metal furnace: $U_{sec} = 133\ V$, $L = 3.82\ \mu H$ and $r = 0.1\ m\Omega$. The momentaneous current is then given by a first order integration of the circuit eqution:

$$\sqrt{2}\, U_{\text{sec}} \cos(\omega t) = L\frac{di}{dt} + r\, i + u_{\text{arc}}, \quad \omega = 2\pi f, \quad f = 50Hz \tag{6}$$

where $u_{arc}(t)$ is the calculated arc voltage which includes the *induced* voltage due to the strong magnetic field in the arc region. This is taken into account by considering the magnetic flux through the modelling domain:

$$u_{\text{arc}} = \int_0^H E_z(r=0)\, dz - \frac{d}{dt}\int_A\int B_\theta\, drdz + U_{an} + U_{ca} \tag{7}$$

U_{an} and U_{ca} are the anode and cathode fall voltages. These are modelled as step-functions which follow the change of polarity of the elctrodes.

To facilitate the discussion of the simulation results the well-known static electric characteristics of the furnace could be used. Despite the fact that the non-linearity of the arc resistance and thus higher harmonics are neglected, which means that the reactance is determined only by the fundamental frequency (X = ωL), the traditional characteristics are useful when discussing trends in the simulation results. Thus the rms current can be expressed as a function of an "effective" arc resistance, R_{arc} :

$$I = U_{\text{sec}} / \sqrt{(R_{\text{arc}} + r)^2 + X^2} \tag{8}$$

The rms arc voltage, the arc power and the total power per phase are then also given as functions of the arc resistance by $U_{arc} = R_{arc}\, I$, $P_{arc} = R_{arc}\, I^2$, $P_{tot} = (R_{arc} + r)\, I^2$.

RESULTS AND DISCUSSION

The conservation equations (1)-(4) together with the equation for the magnetic field (5) are solved with the proper boundary conditions (Table 1). The temperature, velocity, current density, magnetic field and pressure variations in the calculation domain are thereby obtained as functions of time over several AC periods.

Among the input parameters required by the model, the current density at the cathode, $j_c(r)$, and the anode and cathode falls, U_{an} and U_{ca}, must be estimated. In addition a reasonable *arc length* H must be assumed. H will not be constant in a real furnace because of electrode movement, depression of the melt and arc motion and instabilities. In order to evaluate the effect of variations in the cathode current density and the anode and cathode falls, calculations are carried out for $H = 10\ cm$ with parameters as listed in Table 2. An example of the calculated current and voltage, u_{arc}, together with the given transformer voltage versus time is shown in Figure 6 (case C). A time delay between the transformer voltage and the arc voltage and current is observed due to the inductance in the circuit.

TABLE 2. *Parameters used in the calculations and the main results obtained*

H = 10 cm	U_{arc} (V)	I (kA)	P_{tot}(MW)	$P_{radiation}$(%)	$P_{electron\ impact}$(%)
A: $j_c = 2.0 \cdot 10^7$ A/m^2 $U_{an} = U_{ca} = 7.5$ V	118	38.0	4.3	46	10
B: $j_c = 1.0 \cdot 10^7$ A/m^2 $U_{an} = U_{ca} = 7.5$ V	106	55.6	5.6	48	12
C: $j_c = 0.5 \cdot 10^7$ A/m^2 $U_{an} = U_{ca} = 7.5$ V	90	69.9	5.9	53	14
D: $j_c = 1.0 \cdot 10^7$ A/m^2 $U_{an} = U_{ca} = 2.5$ V	100	62.7	6.0	53	8

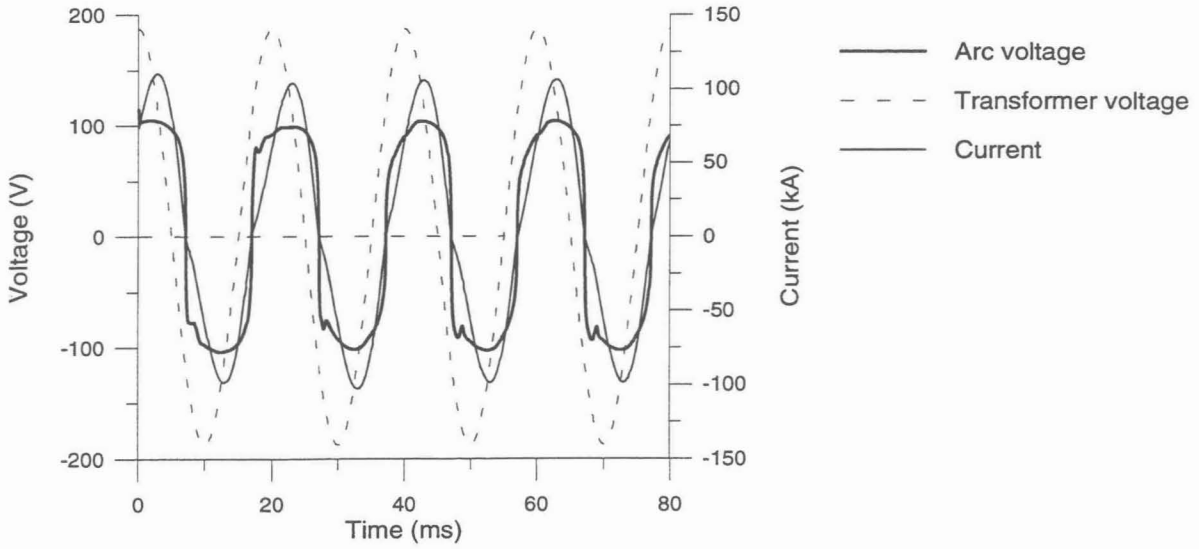

Figure 6 *Calculated current and voltage versus time together with the given transformer voltage (case C, see Table2)*

The rms current, rms arc voltage, total power and arc power per phase *as a function of arc resistance* are calculated as explained above and shown in Figure 7. The total *measured* power of the furnace is 22 MW and assuming symmetric furnace conditions the power per phase will be ~ 7.3 MW, which gives an arc power of ~ 6.7 MW (marked with O on the figure). The rms current and arc voltage is then ~77 kA and ~ 88 V. The calculation results obtained with parameters as listed in Table 2 will be discussed on the basis of this figure.

A value often used for the mean current density on a graphite electrode is $j_c \sim 4 \cdot 10^7$ *A/m*^{2} /11/. This value is obtained from observations of the size of the cathode spot at different AC currents in the range of 4-8 kA and has also been used in this model when simulating arcs at about 1000 A /7/. However, using this value for high-current arcs at ~100 kA gives extremely high temperatures in front of the cathode (T > 30000 K), which seem to be unrealistic. The cathode current density should be different in the two half periods depending on whether the graphite or the melt is cathode, but this is not accounted for in the model. The calculated power from the simulations A, B and C with current densities in the range $0.5 - 2 \cdot 10^7$ *A/m*^{2} are marked in Figure 7. Comparing the calculated and the measured power, the best results are obtained by using the lowest current density. By decreasing the cathode current density,

the temperatures in front of the cathode decreases. Although this gives a lower electric conductivity as seen from Figure 3b), the increased conducting area results in a reduction of the arc resistance and thereby a shift to higher arc power. The value of the cathode current density is thus seen to be a crucial parameter in the simulations.

In future modelling work a more sophisticated sub-model of the cathode sheath should be implemented. The cathodic current density as well as the cathode fall voltage would then be calculated taking into account the material properties of graphite and silicon.

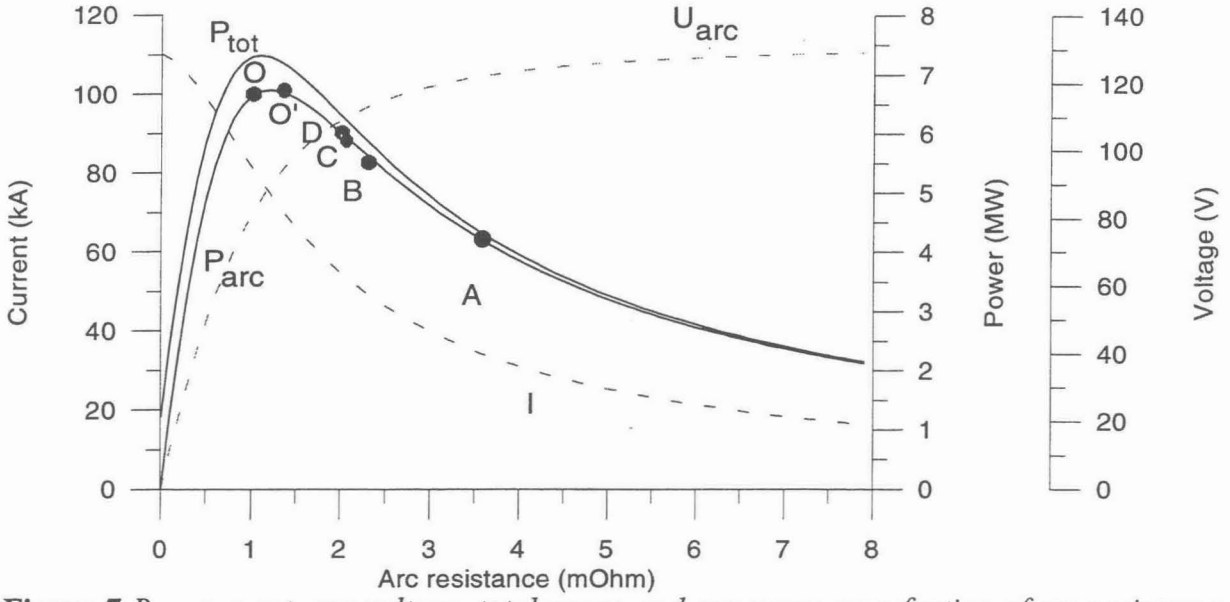

Figure 7 *Rms current, arc voltage, total power and arc power as a funtion of arc resistance*

The values for anode and cathode falls vary from ~ 10 V for argon arcs with currents of some hundred amperes /12/ to 30-40 V in steel furnace arcs /13/. It may also vary during a half period as found by Jordan et al. /11/. AC arcs with currents in the range of 4-8 kA in a steel furnace were investigated and the sum of anode and cathode fall were estimated to vary from 40-50 V just after zero current to 10 V at the end of a half cycle. A reduction of the sum of anode and cathode falls from 15 V (point B) to 5 V (point D) in the model gave an increased current and a reduced arc voltage as expected from the circuit equation (6) - (7).

The effect of turbulence was investigated by using the k-ε model on case D. The rms voltage decreased by 2.3%, whereas the rms current increased by 5.4%. The resulting arc resistance decreased, and the arc power increased by 1.9%. Turbulence, therefore, does not seem to have any significant influence on the modelling results.

When comparing the measured and the calculated arc power one must have in mind that the real arc power may be lower than indicated by point O. Some of the current - eg. 10% - will probably pass through the charge causing the arc power to shift to point O' indicated on Figure 7. To adjust for this a *resistance in parallell with the arc* could be included in the circuit equation. The objection is that we then introduce another uncertain input parameter which is difficult to estimate.

The mean radition power given in Table 2 is seen to depend on the cathode current density. Although the temperature level decreases with decreased cathode current density, the percentage of radiation is seen to increase. Because of the lower current density at the cathode, the Lorentz force is reduced and thereby also the velocities in the arc. The result is a lower

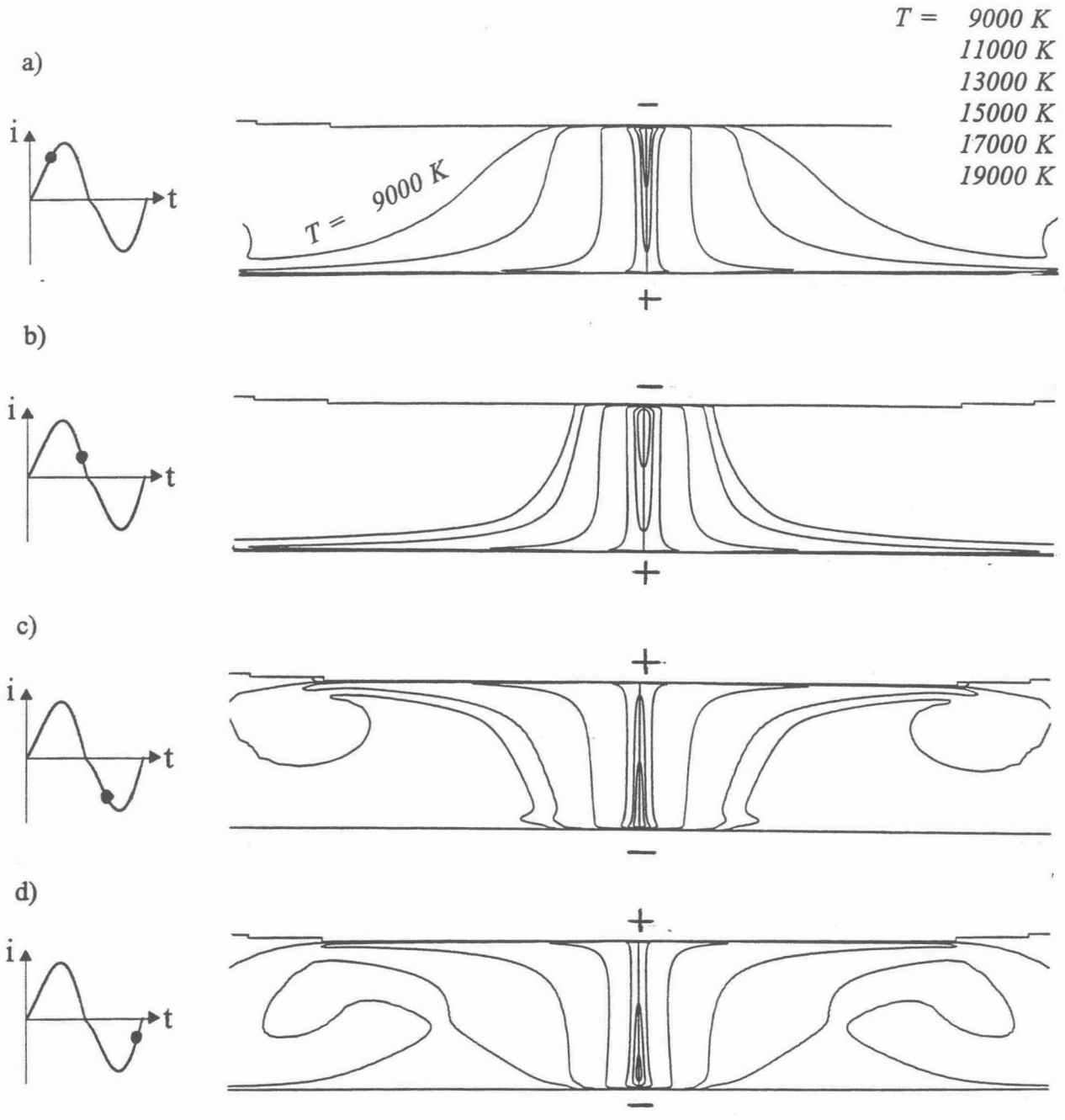

Figure 8 *Contours of constant temperature at different times a) t = 41 ms, i = 86 kA, b) t = 46 ms, i = 43 kA, c) t = 51 ms, i = - 79 kA, d) t = 56 ms, i = - 42 kA. The momentaneous current is indicated on the inserted current vs time diagrams.*

convective heat loss from the arc to the sourrounding surfaces. The energy transferred to the anode by the electrons is from Table 2 seen to increase with increased rms currents in the arc and is also directly proportional to the anode fall. The induced voltage due to the time-varying magnetic flux (7) counts for only 1-2 % of the total arc voltage.

The calculated temperature field at four different instants of time for case C is shown in Figure 8. This illustrates the periodic behaviour of the arc. The axial velocities (left) together with the pressures (right) at the same four time steps are shown in Figure 9. The pressure shown is not the absolute pressure, but the *relative* pressure referred to a point on the crater wall EA in the modelling domain (Figure 1) where the pressure is assumed to be only slightly above 1 bar.

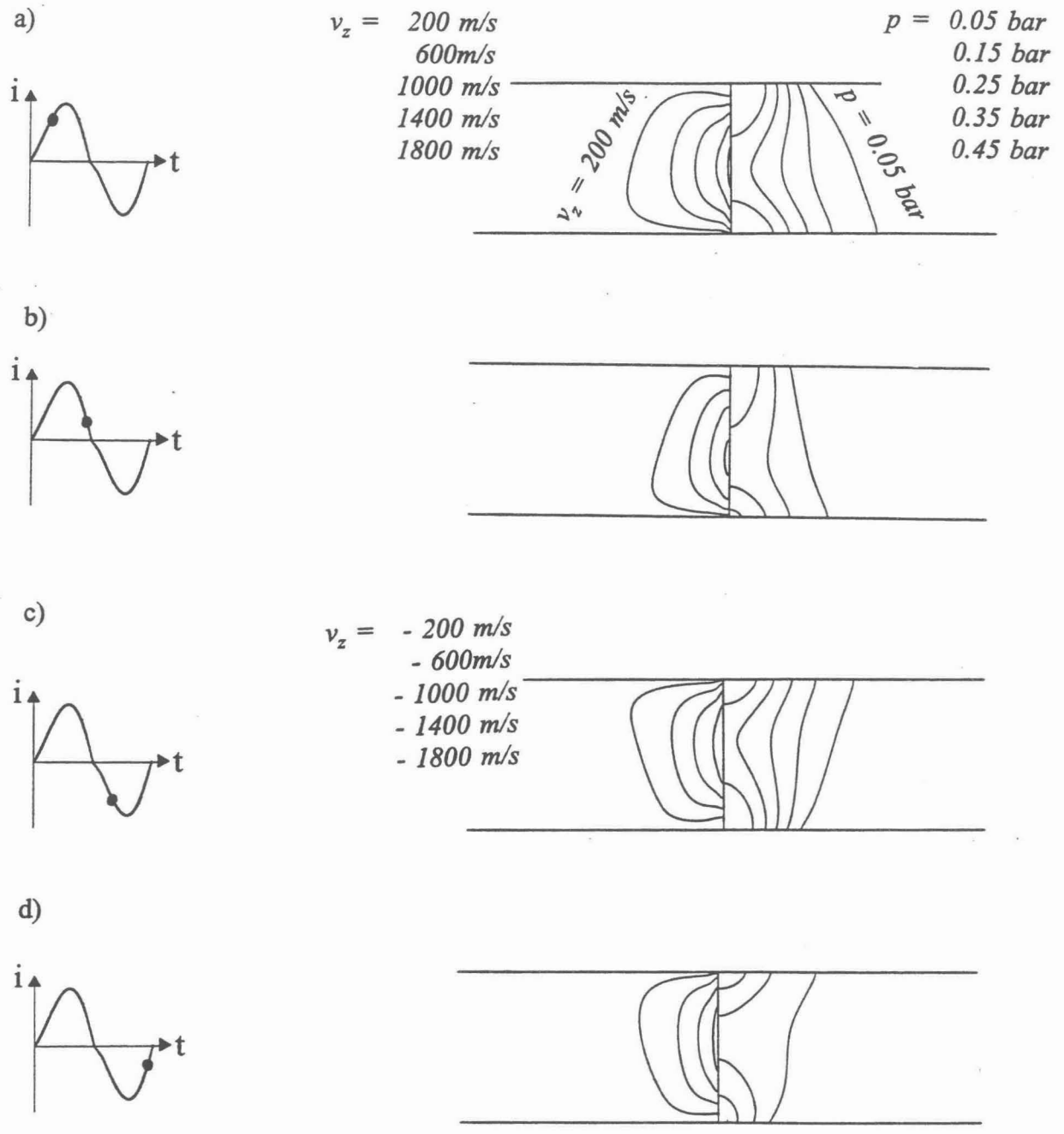

Figure 9 *Contours of constant axial velocity (left) and pressure (right) at different times. a) t = 41 ms, i = 86 kA, b) t = 46 ms, i = 43 kA, c) t = 51 ms, i = - 79 kA, d) t = 56 ms, i = - 42 kA. The momentaneous current is indicated on the figure.*

The high pressure near the cathode is due to the electromagnetic force arising from the interaction of the arc current with its own magnetic field. This force is strongest close to the cathode where there is a radial current component associated with the arc contraction towards the cathode. The axial current density is high for the same reason. A high pressure zone occurs also near the anode because of the stagnation flow in this region. The axial force component $F_z = j_r B_\theta$ accellerates the gas towards the anode and give rise to velocities which may be supersonic as also found by Bowman /12/. The pressure variations should therefore be taken into account in the transport coefficients, thermodynamic data and radiation data used in the simulations. To use data for p = 1 bar seems to be an over-simplification when dealing with the high-current arcs considered here.

CONCLUSION

A numerical model for an AC free-burning arc in a silicon metal furnace is established. Thermodynamic properties and transport coefficients for argon at atmospheric pressure are used in the present simulations. The pressure in the arc is, however, found to be considerably higher than 1 bar and the pressure dependence of transport coefficients, thermodynamic properties and radiation data for Si-O-C crater gas mixtures should therefore be implemented in the model. The most important model parameters which must be estimated are the cathode current density and the anode and cathode fall voltages. Satisfactory agreement between measured and calculated arc current, voltage and power is obtained together with detailed information about the interior structure of the arc. The flow field generated by the arc in the crater is computed, and the relative importance of heat transfer by radiation, electron impact and convection determined. These transport phenomena are crucial for the chemical processes in the crater zone.

ACKNOWLEDGEMENTS

This work has been supported by The Research Assosiation of the Norwegian Ferroalloys Industry (FFF) and the Royal Norwegian Research Council (NFR). The DC model, which forms a part of the AC model presented in this work was developed by A.E. Arntsberg, The Norwegian Institute of Technology. Elkem Fiskaa is thanked for information about the silicon metal furnace.

REFERENCES

/1/ Andresen, B., Tuset, J.K; *Dynamic model for the high-temperature part of the carbothermic silicon metal process*, 7th International Ferroalloys Congress, Trondheim, Norway, 11-14 June, 1995

/2/ Halvorsen S.A., Schei A., Downing, J.H; *A unidimensional dynamic model for the (ferro) silicon process,* 50th Electric Furnace Conference Proceedings, ISS/AIME, Atlanta, USA, 1992

/3/ Schei, A., Larsen, K.; *A stoichiometric model of the ferrosilicon process*, 39th Electric Furnace Conference Proceedings, ISS/AIME, Houston, USA, 1981

/4/ Schäfer, J., Mühlbauer, A.; *Energieumsetzung in Silicium Reduktionsöfen*, Elektrowärme International, Vol. 43, B5, 1985

/5/ Sakulin, M.; *Das Betriebsverhalten des Lichtbogenofen am Netz, 9,* UIE Congres, Cannes, Oct., 1980

/6/ Valderhaug, A. M; *Modelling and control of submerged-arc ferrosilicon furnaces*, Ph.D. thesis, Dept. of Technical Cybernetics, The Norwegian Institute of Technology, 1992

/7/ Larsen, H. L., Bakken, J.A; *A time dependent numerical model for an AC electric arc*, 3rd European Congress on Thermal Plasma Processes, Aachen, Germany, Sept., 1994

/8/ Fluent User Manual, Version 2.9 update, Creare Inc., UK, 1987

/9/ *Thermal Plasmas*, International Summer School on Plasma Chemistry, Editor: S. Veprek, Aug. 31-Sept. 4, 1987, Tokyo, Japan

/10/ Gu, L.; *Thermodynamic and transport properties of and diffusion in (Ar-) Si-O-C plasma mixtures*, SINTEF Materials Technology report, STF24 A94546, 1994

/11/ Jordan, G. R., Bowman, B., Wakelam, D.; *Electrical and photographic measurements of high-power arcs*, J. Phys. D: Appl. Phys., Vol. 3, 1970

/12/ Hsu, K. C., Etemadi, K, Pfender, E.; *Study of the free-burning high intensity argon argon arcs*, J. Appl. Phys., Vol. 54, No. 3, 1983

/13/ Ahlers, H.; *Experimentelle und theoretische Untersuchungen von frei brennenden Gleichstromlichtbögen bis 12 MW an Elektrostahlöfen*, Dissertation der Universität der Bundeswehr Hamburg, 1988

/14/ Bowman, B.; *Properties of arcs in DC furnaces*, 42nd Elecric Furnace Conference Proceedings, ISS/AIME, Nashville, USA, Nov., 1994